JACS
JOURNAL OF THE AMERICAN CHEMICAL SOCIETY

Communication

pubs.acs.org/JACS

Side Chain Dynamics of Carboxyl and Carbonyl Groups in the Catalytic Function of *Escherichia coli* Ribonuclease H

Kate A. Stafford,[†] Fabien Ferrage,[‡] Jae-Hyun Cho,[§,*] and Arthur G. Palmer, III*[,†]

[†]Department of Biochemistry and Molecular Biophysics, Columbia University, New York, New York 10032, United States
[‡]Ecole Normale Supérieure, Département de Chimie, UMR 7203 CNRS-UPMC-ENS, 75005 Paris, France
[§]Department of Biochemistry and Biophysics, Texas A&M University, College Station, Texas 77843-2128, United States

Supporting Information

ABSTRACT: Many proteins use Asx and Glx (x = n, p, or u) side chains as key functional groups in enzymatic catalysis and molecular recognition. In this study, NMR spin relaxation experiments and molecular dynamics simulations are used to measure the dynamics of the side chain amide and carboxyl groups, $^{13}C^{\gamma/\delta}$, in *Escherichia coli* ribonuclease HI (RNase H). Model-free analysis shows that the catalytic residues in RNase H are preorganized on ps−ns time scales via a network of electrostatic interactions. However, chemical exchange line broadening shows that these residues display significant conformational dynamics on μs−ms time scales upon binding of Mg^{2+} ions. Two groups of catalytic residues exhibit differential line broadening, implicating distinct reorganizational processes upon binding of metal ions. These results support the "mobile metal ion" hypothesis, which was inferred from structural studies of RNase H.

Understanding protein dynamics is critical for elucidating the molecular mechanisms of many biological processes, including enzyme catalysis and protein−protein interactions.[1−3] Recent developments in NMR spin relaxation methods have enabled the investigation of biomolecular dynamics in atomic detail.[4−7] Nonetheless, despite the importance of Asx and Glx residues in enzyme catalysis and substrate binding processes, surprisingly few studies on the side chain dynamics of these residues have been reported.[8−10] Here, we present a $^{13}C^{\gamma/\delta}$ relaxation investigation of the side chain amide and carboxyl groups in Asx/Glx residues of *E. coli* RNase H, by using recently developed NMR relaxation methods.[8] To gain more mechanistic insights, we have compared our experimental findings with the results of molecular dynamics (MD) simulations. RNase H cleaves the RNA strand of a RNA/DNA hybrid (Figure 1).[11] The active site includes four acidic residues (D10, E48, D70, and D134) that require Mg^{2+} ions for catalytic activity.[12−14] Experimental and simulated side chain generalized order parameters, S^2, which represents the mobility of the C−C′ bond vector in the side chain amide and carboxyl groups of Asx/Glx residues, including the catalytic residues, provide direct evidence of preorganization of the catalytic residues on ps−ns time scales. However, these preorganized catalytic residues show significant conformational dynamics on μs−ms time scales, which might be required for reorganizing the catalytic groups upon sequential binding of metal ions.

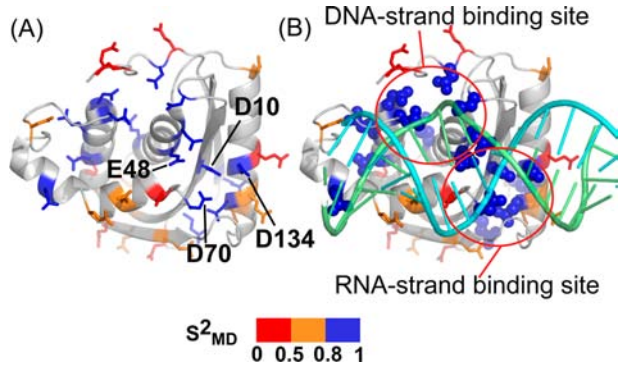

Figure 1. (A) Ribbon representation of RNase H (PDB ID 2RN2). All Asx/Glx residues are shown as stick models and color-coded based on the value of S^2_{MD}. Key catalytic residues are labeled. (B) Structure of RNA/DNA hybrid substrate from the human RNase H complex (PDB ID 2KQ9) is superimposed onto *E. coli* protein (PDB ID 2RN2). The most rigid side chains are shown as space-filling models. DNA and RNA strands are shown in green and cyan, respectively.

Residue-specific values of S^2 were determined using the model-free formalism applied to longitudinal (R_1) and cross-correlated transverse (η_{xy}) relaxation rate constants of the $^{13}C^{\gamma/\delta}$ nuclei.[8] The chemical shift anisotropy (CSA) tensors for carbonyl and carboxyl $^{13}C^{\gamma/\delta}$ are highly asymmetric and depend upon the local environment.[15] For carbonyl ^{13}C, we used the average backbone carbonyl $^{13}C'$ CSA values determined for GB1 using solid-state NMR spectroscopy: δ_{xx} = 240.87 ppm, δ_{yy} = 196.62 ppm, and δ_{zz} = 93.5 ppm.[15] For carboxyl ^{13}C, δ_{xx} = 242 ppm, δ_{yy} = 191 ppm, and δ_{zz} = 105 ppm were assumed.[16] The model-free analysis was also repeated with extreme CSA values of the carbonyl and carboxyl ^{13}C spins to test the stability of the results (see Supporting Information, SI). We were able to analyze relaxation rates for 22 of the 34 Asx/Glx residues. Many of the excluded residues from the analysis are well-exposed to the solvent in the structure and showed very slow development of the cross peaks through cross-correlated relaxation; additional details of experiments and the model-free analysis are described in SI.

To complement experimental studies with direct observations of side chain dynamics, we performed MD simulations of *E. coli* RNase H initiated from the crystal structure (PDB ID

Received: September 12, 2013
Published: November 13, 2013

   dx.doi.org/10.1021/ja409479y | J. Am. Chem. Soc. 2013, 135, 18024−18027

2RN2) protonated in accordance with experimental pK_a measurements[13] to reflect pH values of 5.5 and 8.0. The protein was described with the Amber99SB force field,[17] solvated in TIP3P water, and neutralized with Cl^- ions. Simulations of 100 ns duration were performed using Desmond Academic release 3 or source release 2.4.2.1.[18] Experimental- (S^2_{NMR}) and MD-derived (S^2_{MD}) side chain order parameters showed significant correlation (R^2 = 0.72 and rmsd = 0.11) (Figure 2A), allowing us to use S^2_{MD} to infer the mechanistic details of dynamics in the ps−ns time scale.

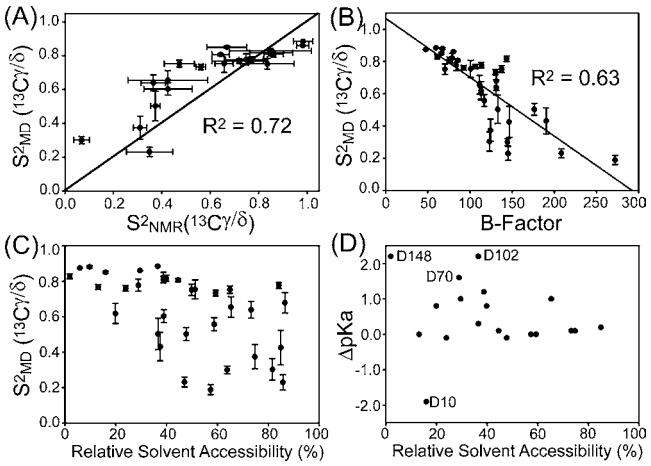

Figure 2. (A) Comparison of order parameters between the experiment (S^2_{NMR}) and simulation (S^2_{MD}). (B) Correlation plot between S^2_{MD} and crystallographic B-factor for side chains (PDB ID 2RN2). The B-factors are the sum of side chain heavy atoms (C, N, and O). (C) S^2_{MD} vs relative solvent accessibility (RSA) of the side chain calculated from the crystal structure of RNase H (2RN2). RSA was calculated using GetArea.[25] (D) Correlation plot between RSA and ΔpK_a. The ΔpK_a for D148 and D102 was estimated by assuming pK_a = 2.0.[13] Corresponding graphs with S^2_{NMR} are shown in SI.

Order parameters of Asx/Glx side chains showed a broad spectrum of dynamics and were uncorrelated with backbone N−H bond mobility (see SI). Values of S^2_{MD} correlate reasonably well with crystallographic B-factors of the side chains, despite the differences in the nature and time scale of the motions detected by each parameter (Figure 2B). On the contrary, S^2_{MD} is poorly correlated with relative solvent accessibility (RSA) of the side chains (Figure 2C). Recent analysis of order parameters for K side chain amino groups showed strong correlations with both crystallography B-factors and RSA of side chain amino groups.[19] This difference suggests that the side chains of Asx/Glx interact more strongly with other parts of the protein because of a shorter side chain length relative to K. Notably, perturbations of pK_a, relative to intrinsic values, do not linearly correlate with solvent accessibility of side chains for Asp or Glu (Figure 2D). With the exception of residue D70, pK_a's are close to intrinsic values for residues with RSA > 50% but become highly heterogeneous for larger degrees of burial. The unusual perturbations of pK_a for D10 and D70 reflect coupling arising from close spatial proximity in the active site.[13]

Overall, MD simulations showed that the side chains of D ($S^2_{MD,ave}$ = 0.87 ± 0.08) and N ($S^2_{MD,ave}$ = 0.85 ± 0.08) residues are the most rigid, followed by E ($S^2_{MD,ave}$ = 0.64 ± 0.21) and Q ($S^2_{MD,ave}$ = 0.46 ± 0.21) residues. S^2_{MD} values were used to obtain unbiased statistics because experimental data do not include S^2_{NMR} values of highly flexible residues. Nonetheless, the same pattern was observed with the experimental S^2_{NMR} values. A previous study on the side chain dynamics of calbindin D_{9k} showed similar statistics for each amino acid type.[8] It is possible that this effect is primarily due to side chain length; however, functional group rigidity is not necessary correlated to overall side chain entropy.[20] Our data provide additional experimental evidence that the side chain of D is usually more rigid than that of E and support the hypothesis that the higher rigidity of the D side chain favors this residue in enzyme active sites.[21]

Rigid side chains are mainly located in the active site of RNase H, which binds to the RNA strand, and the interface with the DNA strand of the RNA/DNA hybrid substrate (Figure 1B). Experimental (simulation) S^2 values of $^{13}C^{\gamma/\delta}$ for D10, E48, D70 and D134 are 0.67 ± 0.08 (0.85 ± 0.01), 0.72 ± 0.11 (0.76 ± 0.01), 0.75 ± 0.09 (0.78 ± 0.03), and 0.64 ± 0.04 (0.81 ± 0.01), respectively. Our NMR experiments were performed at pD = 6.2, which is close to the pK_a of D10 (6.1).[13] Therefore, experimental S^2 values of the catalytic residues represent the average mobility of D10 in protonated and deprotonated states. High rigidity of the catalytic residues is also suggested by low crystallographic B-factors determined under conditions where D10 would be deprotonated (pH > 8.8; PDB ID 2RN2).[22] Because we calculated S^2_{MD} values with D10 in the protonated state and other acidic residues in the deprotonated state, we further tested if D10 remains rigid at high pH by running another simulation with deprotonated D10. During the simulation, we observed that deprotonated D10 forms a water-mediated hydrogen bond with D134 and remains highly rigid (S^2_{MD} = 0.847 ± 0.002). Discrepancies in S^2 values for active site residues may reflect inability of standard molecular mechanics force fields to model changes in protonation state and not incomplete conformational sampling alone. The crystal structure of Mg^{2+}-bound RNaseH (PDB ID, 1RDD) shows relatively minor conformational change of the catalytic residues, relative to the apo state (PDB ID 2RN2)[23](see SI). Therefore, our data indicate that the catalytic residues in RNaseH are preorganized to minimize entropy penalties upon coordinating Mg^{2+} for catalysis.[24]

The net free energy change, ΔG, from electrostatic interactions of the acidic residues, D and E, can be calculated from the pK_a shift relative to intrinsic pK_a (Figure 3A). The free energy is the sum of three terms: $\Delta G = \Delta H_{bind} - T(\Delta S_{sol} + \Delta S_{conf})$, in which ΔH_{bind} is the enthalpy change and ΔS_{sol} and

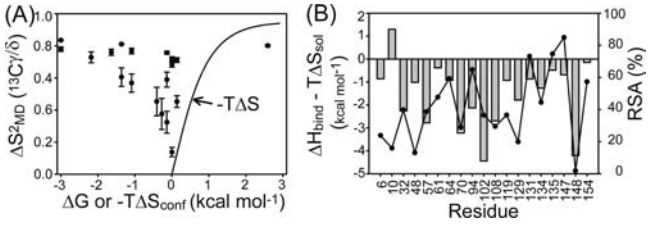

Figure 3. (A) Plot of S^2_{MD} vs ΔG associated with the changes in pK_a of each acidic residue. Solid line represents $-T\Delta S_{conf}$.[26] For calculation of $-T\Delta S_{conf}$, the order parameter was assumed to change from 0.05 to each S^2_{MD} value (i.e., $\Delta S^2_{MD} = S^2_{MD} - 0.05$). (B) Calculated $\Delta H_{bind} - T\Delta S_{sol}$ (bars) and relative solvent accessibility (closed circles) for each acidic residue. Uncertainties for the reported pK_a values are not available so the calculated $\Delta H_{bind} - T\Delta S_{sol}$ do not include uncertainties. Plots with the experimental order parameters are shown in SI.

dx.doi.org/10.1021/ja409479y | J. Am. Chem. Soc. 2013, 135, 18024−18027

ΔS_{conf} are the entropy changes associated with solvent and protein conformational changes, respectively. The contribution of $-T\Delta S_{conf}$ to the free energy can be estimated from ΔS^2.[26,27] Figure 3B presents $-T\Delta S_{conf}$, which was calculated as shown by Yang and Kay.[26] The horizontal distance between each data point and the calculated $-T\Delta S_{conf}$ line is an estimate of $\Delta H_{bind} - T\Delta S_{sol}$ provided by salt bridge formation (Figure 3B). This plot shows that the magnitudes of the local electrostatic interactions are highly heterogeneous.[28,29] One group of residues has $-0.5 \leq \Delta G \leq 0$ kcal/mol and the entropic penalty $-T\Delta S_{conf}$ nearly offsets the favorable contributions from $\Delta H_{bind} - T\Delta S_{sol}$. A second set of residues has $\Delta G \leq -1$ kcal/mol with large favorable contributions from $\Delta H_{bind} - T\Delta S_{sol}$ that offset the entropic penalty, despite the high rigidity of side chains in this group. Residue D10 is the only residue in the third group, having a positive value of ΔG, again reflecting interactions with D70 in the active site. These data indicate that the measurement of the side chain entropy of acidic residues can be critical for understanding the role of electrostatic interactions in biological processes. Although not considered in this analysis, $-T\Delta S_{conf}$ of the interacting partner molecule should also be determined for better estimation of $\Delta H_{bind} - T\Delta S_{sol}$. We tested whether the differential burial of charged residues generates the heterogeneity in $\Delta H_{bind} - T\Delta S_{sol}$. Interestingly, solvent accessibility of salt bridges only weakly correlates with $\Delta H_{bind} - T\Delta S_{sol}$ (R^2 = 0.12) (Figure 3B), indicating that the geometry of the salt bridge may be more critical for its stability.[29] Similar approaches using backbone and methyl-bearing side chains highlighted the role of conformational entropy in ligand binding.[6,26,27,30] Because individual free energy changes upon salt bridge formation can be directly measured using ΔpK_a, acidic side chain order parameters enable the site-specific analysis of energetic contribution of conformational dynamics. This is an additional benefit compared to the analysis using order parameters for backbone or methyl-bearing side chains.

The $^{13}C^{\gamma/\delta}$ order parameters become extremely heterogeneous as side chains become more exposed to the solvent (RSA > 35%). Although buried residues (RSA < 20%) tend to have high S^2 values, many partially or fully solvent-exposed residues also have high S^2 values (Figure 2C). For example, E57 and R106 form a solvent-exposed salt bridge, which results in high rigidity for the side chains of both residues. By contrast, D102 and R46 form a completely buried salt bridge and also showed high rigidity for both interacting side chains.[20] This indicates that solvent-exposed salt bridges and hydrogen bonds can restrict the motion of the C−C′ bond as effectively as completely buried salt bridges. The partially solvent-exposed D134 (RSA = 44.5%) forms a salt bridge with R138, resulting in high-order parameters for both residues. The D134-R138 salt bridge is strong enough to offset 1.13 kcal mol^{-1} entropic penalty from $-T\Delta S_{conf}$, giving $\Delta G \approx 0$. When the enzyme−substrate (ES) complex is formed, this salt bridge breaks, D134 coordinates a metal ion for catalysis, and R138 interacts with the phosphodiester bond of the RNA/DNA substrate to stabilize the ES complex. Therefore, the entropic cost of forming the ES complex may be minimized by preordering these two side chains. This example illustrates the insights provided by side chain order parameters into the molecular origins of the specificity and binding affinity of proteins.

The RNase H family is found in nearly all organisms, from viruses to human. We investigated if side chains with high S^2 values are evolutionary conserved (see SI). Interestingly, the most conserved Asx/Glx residues are D10, N16, N45, E48, D70, N130, E131, and D134, all of which have high S^2 values (>0.8). The rigidity of N45 and N130 is particularly notable because these residues interact with the substrate in the *H. sapiens* complex and are located within 4 Å of the active-site catalytic residues. However, not all residues with high values of S^2 are well conserved. For example, E6 forms a partially buried salt bridge with R27 in *E. coli* RNase H. Replacement of E6 by a hydrophobic residue, V in human RNase H, is accompanied by replacement of R27 by a hydrophobic residue, also V in human RNase H (see SI). Diverse functional roles of buried salt bridges have been described in other contexts.[31−33] Waldburger et al. reported that replacement of a salt bridge network by hydrophobic residues increases the stability of the Arc repressor but changes binding cooperativity.[32] RNase H exists as a separate entity in *E. coli*, whereas it is part of multidomain protein in many other organisms including human. Thus, dissection of the role of buried electrostatic interactions should be considered in the context of full-length proteins and not just isolated domains.

Despite many structural and biochemical studies, the details of Mg^{2+} binding and coordination in the active site of RNase H are not completely understood.[12,34,35] Figure 4A shows the

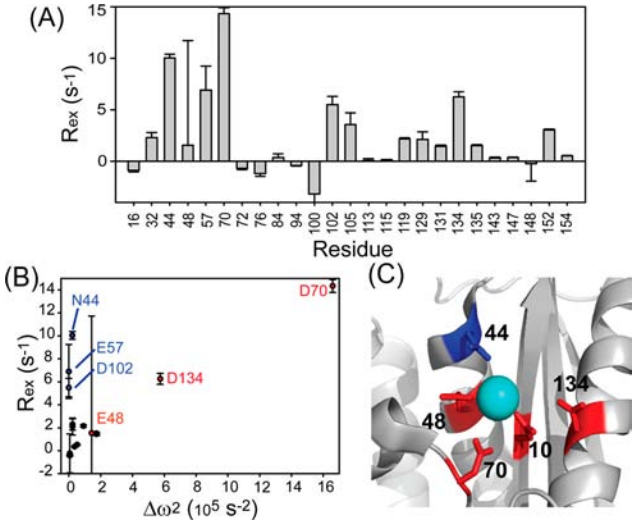

Figure 4. (A) Contribution of μs−ms time scale dynamics, R_{ex} (= $R_{1\rho}^{Mg} - R_{1\rho}^{apo}$, upon binding of Mg^{2+} to the active site. The D10 peak was too broadened to measure. The spin-lock RF amplitude was $\omega_{SL}/2\pi$ = 1.1 kHz (see SI). (B) Correlation plot between R_{ex} and the squared chemical shift differences, $\Delta\omega^2$, between apo and Mg^{2+}-bound states. The residues that belong to groups 1 and 2 are labeled in blue and red, respectively. (C) Ribbon representation of the active site of RNase H (PDB ID 1RDD). Groups 1 and 2 residues are color coded according to panel B. Only active site residues are shown for clarity. The Mg^{2+} ion is shown as a cyan sphere.

effects on $^{13}C^{\gamma/\delta}$ line widths from chemical exchange on the μs−ms time scale associated with Mg^{2+} binding processes determined from $R_{1\rho}$ data acquired with and without Mg^{2+}. Catalytic residues in the active site, except E48, showed significant $R_{ex} = R_{1\rho}^{Mg} - R_{1\rho}^{apo}$. To determine if the observed $^{13}C^{\gamma/\delta}$ dynamics represent the same motional process, we plotted R_{ex} versus squared chemical shift differences, $\Delta\omega^2$, between apo and Mg^{2+}-bound RNase H. Assuming a fast exchange process, residues with nonzero R_{ex} are expected to belong to a single correlation line between R_{ex} and $\Delta\omega^2$ if the

dx.doi.org/10.1021/ja409479y | J. Am. Chem. Soc. 2013, 135, 18024−18027

residues experience the same conformational exchange process. The pK_a of some residues are changed upon binding of Mg^{2+}; however, the pK_a shifts do not affect R_{ex} (see SI). Interestingly, we found two distinct groups of residues showing differential dynamics in response to Mg^{2+} binding (Figure 4B,C). Group 1 consists of N44, E57, and D102, and group 2 consists of D10, E48, D70, and D134. E48 has large uncertainty because of low signal-to-noise ratio in Mg^{2+}-bound state. We included D10 in group 2 because R_{ex} was too large to be measured, and this residue has the largest chemical shift difference ($\Delta\omega^2 = 45.0 \times 10^5\ s^{-2}$) between apo and Mg-bound RNase H, consistent with the proposed role of D10 as a major metal ion-coordinating residue.

RNase H has been proposed to coordinate two Mg^{2+} ions for catalysis,[14,34] although only a single Mg^{2+} ion was found in the active site in the absence of substrate.[23] According to the substrate-bound structure of human RNase H (the two Mg^{2+} ion model), the A-site consists of D10 and D134, while the B-site consists of D10, D70, and E48.[14] Proper binding of the substrate is essential for promoting the coordination of two Mg^{2+} ions in the active site.[14] Moreover, the position of metal ion in the active site may be highly heterogeneous (see SI) and mobile depending on the catalytic step.[12,14,35] The difference in μs−ms time scale dynamics between groups 1 and 2 may indicate that the binding of the first Mg^{2+} can trigger conformational dynamics of the residues required for coordinating the second Mg^{2+} ion and substrate. Complex interplay among active site residues upon binding of metal ions was also proposed based on structural analysis of Mn^{2+}-bound RNase H.[12] However, our current data do not distinguish whether the observed μs−ms time scale dynamics of the group 1 residues is induced by the binding of the first Mg^{2+} ion to the group 2, or whether metal ion binding changes the chemical environment in a way that hidden, but already present, dynamics become observable. In summary, although the catalytic residues of RNase H are highly rigid in the ps−ns time scale, they undergo significant conformational dynamics in the μs−ms time scale upon metal ion binding, which may reflect reorganization of the active site.[24,36]

■ ASSOCIATED CONTENT

Supporting Information

Experimental and simulation details and supporting figures. This material is available free of charge via the Internet at http://pubs.acs.org.

■ AUTHOR INFORMATION

Corresponding Authors

jaehyuncho@tamu.edu
agp6@columbia.edu

Notes

The authors declare no competing financial interest.

■ ACKNOWLEDGMENTS

This research was funded by an NSF graduate research fellowship (K.A.S.) and NIH grant GM50291 (A.G.P.). We thank the Center for Computational Biology and Bioinformatics (C2B2) for computational resources.

■ REFERENCES

(1) Smock, R. G.; Gierasch, L. M. *Science* **2009**, *324*, 198.
(2) Nashine, V. C.; Hammes-Schiffer, S.; Benkovic, S. J. *Curr. Opin. Struct. Biol.* **2010**, *14*, 644.
(3) Boehr, D. D.; Nussinov, R.; Wright, P. E. *Nat. Chem. Biol.* **2009**, *5*, 789.
(4) Boehr, D. D.; McElheny, D.; Dyson, J. J.; Wright, P. E. *Science* **2006**, *15*, 1638.
(5) Mittermaier, A.; Kay, L. E. *Science* **2006**, *312*, 224.
(6) Wand, A. J. *Curr. Opin. Struct. Biol.* **2013**, *23*, 75.
(7) Palmer, A. G. *Chem. Rev.* **2004**, *104*, 3623.
(8) Paquin, R.; Ferrage, F.; Mulder, F. A.; Akke, M.; Bodenhausen, G. *J. Am. Chem. Soc.* **2008**, *130*, 15805.
(9) Hansen, A. L.; Kay, L. E. *J. Biomol. NMR* **2011**, *50*, 347.
(10) Pasat, G.; Zintsmaster, J. S.; Peng, J. W. *J. Magn. Reson.* **2008**, *193*, 226.
(11) Crouch, R. J.; Dirksen, M.-L. *Nuclease*; Cold Spring Harbor Laboratory: Cold Spring Harbor, 1982.
(12) Goedken, E. R.; Marqusee, S. *J. Biol. Chem.* **2001**, *276*, 7266.
(13) Oda, Y.; Yamazaki, T.; Nagayama, K.; Kanaya, S.; Kuroda, Y.; Nakamura, H. *Biochemistry* **1994**, *33*, 5275.
(14) Nowotny, M.; Gaidamakov, S. A.; Ghirlando, R.; Cerritelli, S. M.; Crouch, R. J.; Yang, W. *Mol. Cell* **2007**, *28*, 264.
(15) Wylie, B. J.; Sperling, L. J.; Frericks, H. L.; Shah, G. J.; Franks, W. T.; Rienstra, C. M. *J. Am. Chem. Soc.* **2007**, *129*, 5318.
(16) Gardiennet-Doucet, C.; Henry, B.; Tekely, P. *Prog. Nucl. Magn. Reson. Spectrosc.* **2006**, *49*, 129.
(17) Hornak, V.; Abel, R.; Okur, A.; Strockbine, B.; Roiterg, A.; Simmering, C. *Proteins: Struct. Funct. Bioinf.* **2006**, *65*, 712.
(18) Bowers, K. J.; Chow, E.; Xu, H.; Dror, R. O.; Eastwood, M. P.; Gregersen, B. A.; Klepeis, J. L.; Kolossvary, I.; Moraes, M. A.; Sacerdoti, F. D.; Salmon, J. K.; Shan, Y.; Shaw, D. E. In Proceedings of the 2006 ACM/IEEE conference on Supercomputing, Tampa, FL, November 11−17, 2006; IEEE: New York, 2006, p 84.
(19) Esadze, A.; Li, D. W.; Wang, T.; Brüschweiler, R.; Iwahara, J. *J. Am. Chem. Soc.* **2011**, *133*, 909.
(20) Trbovic, N.; Cho, J. H.; Abel, R.; Friesner, R. A.; Rance, M.; Palmer, A. G. *J. Am. Chem. Soc.* **2009**, *131*, 615.
(21) Bartlett, G. J.; Porter, C. T.; Borkakoti, N.; Thornton, J. M. *J. Mol. Biol.* **2002**, *324*, 105.
(22) Katayanagi, K.; Miyagawa, M.; Matsushima, M.; Ishikawa, M.; Kanaya, S.; Nakamura, H.; Ikehara, M.; Matsuzaki, T.; Morikawa, K. *J. Mol. Biol.* **1992**, *223*, 1029.
(23) Katayanagi, K.; Okumura, M.; Morikawa, K. *Proteins* **1993**, *17*, 337.
(24) Warshel, A. *J. Biol. Chem.* **1998**, *273*, 27035.
(25) Fraczkiewics, R.; Braun, W. *J. Comput. Chem.* **1998**, *19*, 319.
(26) Yang, D.; Kay, L. E. *J. Mol. Biol.* **1996**, *263*, 369.
(27) Akke, M.; Bruschweiler, R.; Palmer, A. G. *J. Am. Chem. Soc.* **1993**, *115*, 9832.
(28) Isom, D. G.; Castañeda, C. A.; Cannon, B. R.; Velu, P. D.; García-Moreno, E. B. *Proc. Natl. Acad. Sci. U.S.A.* **2010**, *107*, 16096.
(29) Kumar, S.; Nussinov, R. *J. Mol. Biol.* **1999**, *293*, 1241.
(30) Tzeng, S. R.; Kalodimos, C. G. *Nature* **2012**, *488*, 236.
(31) Dong, F.; Zhou, H.-X. *Biophys. J.* **2002**, *83*, 1341.
(32) Waldburger, C. D.; Schildbach, J. F.; Sauer, R. T. *Nat. Struct. Biol.* **1995**, *2*, 122.
(33) Xu, D.; Tsai, C.-J.; Nussinov, R. *Protein Eng.* **1997**, *10*, 999.
(34) Yang, W. *Nat. Struct. Mol. Biol.* **2008**, *15*, 1228.
(35) Tsunaka, Y.; Takano, K.; Matsumura, H.; Yamagata, Y.; Kanaya, S. *J. Mol. Biol.* **2004**, *324*, 1171.
(36) Hammes-Schiffer, S. *Biochemistry* **2013**, *52*, 2012.